CARS spectroscopy of O2(1Δg) from the Hartley band photodissociation of O3: Dynamics of the dissociation

James J. Valentini, Daniel P. Gerrity, David L. Phillips, JongChen Nieh, and Kevin D. Tabor

Citation: J. Chem. Phys. **86**, 6745 (1987); doi: 10.1063/1.452374
View online: http://dx.doi.org/10.1063/1.452374
View Table of Contents: http://jcp.aip.org/resource/1/JCPSA6/v86/i12
Published by the American Institute of Physics.

CARS spectroscopy of $O_2(^1\Delta_g)$ from the Hartley band photodissociation of O_3: Dynamics of the dissociation

James J. Valentini, Daniel P. Gerrity,[a] David L. Phillips, Jong-Chen Nieh, and Kevin D. Tabor

Department of Chemistry, University of California, Irvine, California 92717

(Received 29 December 1986; accepted 10 March 1987)

Rotationally and vibrationally resolved CARS spectra of the $O_2(^1\Delta_g)$ photofragment produced by the photodissociation of O_3 at 17 wavelengths between 230 and 311 nm are reported. The spectra are taken under collision-free conditions, therefore, they reveal the nascent rotational and vibrational state distributions of the $O_2(^1\Delta_g)$ photofragment. At all photolysis wavelengths studied the vibrational distribution peaks very sharply at $v = 0$, although all energetically allowed vibrational states are observed. The rotational state distributions are narrow, and peak typically at high J. The rotational distribution shifts to lower J as the photolysis wavelength increases. These observations imply vibrationally adiabatic, rotationally impulsive energy release in the dissociation. The shape and width of the rotational distributions can be completely accounted for by the spread in the O_3 thermal rotation and zero-point vibration contributions to the $O_2(^1\Delta_g)$ photofragment angular momentum. The most striking observation about the $O_2(^1\Delta_g)$ photofragment quantum state distribution is an apparent propensity for even-J states. Experiments with ^{18}O enriched ozone indicate that this propensity is observed only for $^{16}O^{16}O$, not for $^{18}O^{16}O$, and by implication not for $^{17}O^{16}O$. We show that this is the consequence of a selective depletion of only odd-J rotational states of $^{16}O^{16}O(^1\Delta_g)$ by a curve crossing to $O_2(^3\Sigma_g)$, but an equal depletion of both even-J and odd-J rotational states of $^{18}O^{16}O$ and $^{17}O^{16}O(^1\Delta_g)$ by the curve crossing. The odd-J selectivity for $^{16}O^{16}O$ is a consequence of the restriction of $^3\Sigma_g$ to only odd-J states, due to the requirement of even nuclear exchange symmetry for this homonuclear species with spin-zero nuclei. As a result of the different curve crossing behavior, the quantum yield for $^3\Sigma_g$ is twice as great for $^{18}O^{16}O$ and $^{17}O^{16}O$ as it is for $^{16}O^{16}O$, and this imposes a mass-independent isotopic fractionation in the photodissociation: the $O_2(^1\Delta_g)$ fragments are depleted of ^{17}O and ^{18}O, while the $O_2(^3\Sigma_g)$ fragments are enriched in these isotopes.

I. INTRODUCTION

The photochemistry of ozone plays a major role in the atmosphere of the earth, determining in large measure the physical structure and chemical composition of the stratosphere.[1-4] The significance of ozone photochemistry is due in part to the spectral location of the Hartley absorption band, shown in Fig. 1, in the near UV, and to the production of electronically excited products in the primary dissociation,

$$O_3 + h\nu \rightarrow O_2(^1\Delta_g) + O(^1D) \quad (1)$$

$$\rightarrow O_2(^3\Sigma_g) + O(^3P). \quad (2)$$

The best experimental measurements to date indicate[2] a quantum yield of unity for dissociation upon absorption in the Hartley band, with the quantum yield for process (1), the singlet channel, of 0.85 to 0.90 throughout the band, except in the so-called falloff region near the 310 nm energetic threshold for this channel. These same measurements show a quantum yield for the triplet channel, process (2), of 0.15 to 0.10 except near the threshold for the singlet channel.

The Hartley band photodissociaiton of ozone is also of fundamental interest because of the way in which the two product channels arise. *Ab initio* calculations[5] show that two different photofragment electronic states are accessible because of a curve crossing in the photolysis exit channel, not because of absorption to two different O_3 excited states. The section through the O_3 potential surfaces shown in Fig. 2 illustrates this curve crossing. Since curve crossing probabilities are quantum state dependent, we can expect the curve crossing shown in Fig. 2 to have interesting consequences for the photofragment vibrational, rotational, and translational state distributions.

The determination of these photofragment final state distributions in the Hartley band dissociation of ozone is the subject of this publication. We describe the use of coherent anti-Stokes Raman scattering (CARS) spectroscopy to record rotationally and vibrationally resolved spectra of the O_2 photofragments under collision-free conditions, upon photodissociation of O_3 at 17 wavelengths from 230 to 311 nm. This work is motivated by preliminary measurements of this type made previously by one of us.[6] These preliminary experiments revealed an unusual propensity for even rotational states of the $O_2(^1\Delta_g)$ photofragment upon dissociation at 266 nm.

The experiments described here, particularly experiments in which we dissociate ^{16}O,^{18}O isotopically mixed ozone, demonstrate that the curve crossing in the photodis-

[a] Permanent address: Department of Chemistry, Carroll College, Waukesha, Wisconsin 53186.

 0021-9606/87/126745-12$02.10

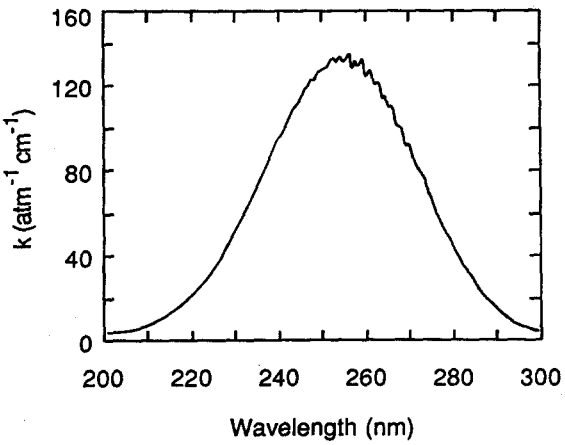

FIG. 1. Hartley band absorption spectrum for O_3, adapted from Ref. 22.

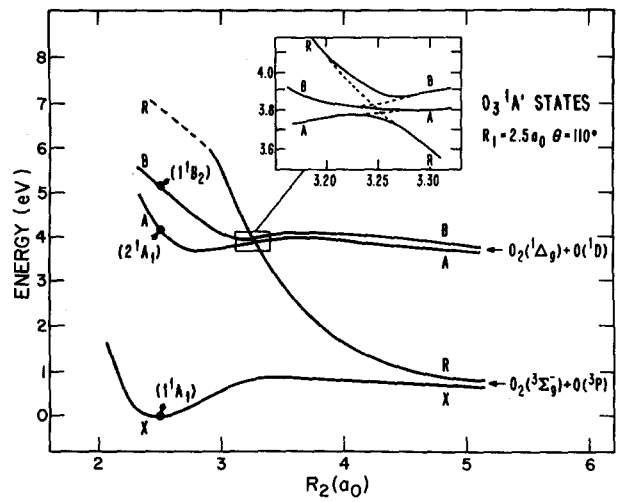

FIG. 2. Section through the low-lying singlet potential energy surfaces of O_3, from Ref. 5. The energy is plotted as a function of one bond length at constant bond angle and constant length for the other bond.

sociation is the source of the even-J propensity observed in the $^1\Delta_g$ spectra. We also show that the curve crossing is isotopically selective, and leads to mass-independent isotopic fractionation of oxygen upon UV photolysis of ozone. This isotopic fractionation may have important consequences for atmospheric chemistry, as well as for cosmochemistry. These consequences are discussed in the following article.[7]

Our experiments also show that the dissociation dynamics of O_3 upon absorption of UV light can be described roughly as vibrationally adiabatic/rotationally impulsive, but the photofragment final state distributions show some deviation from purely impulsive (rotationally) energy release. Semiclassical model calculations of the O_2 fragment rotational distributions indicate that the width and shape of these distributions can be explained by the contribution of O_3 rotation and zero-point bending vibration to the total angular momentum, but only if half of the final rotational states allowed by angular momentum and energy conservation are not produced.[8] The next section describes the experimental methodology and apparatus, while Sec. III presents the experimental results obtained. In Sec. IV we discuss the even-J propensity and show that it is a result of the selection rules governing the $^1\Delta_g + {}^1D/{}^3\Sigma_g + {}^3P$ curve crossing, and also in that section explain the photodissociation dynamics. In the last section we summarize conclusions to be drawn from our results.

II. EXPERIMENTS

Our experiments use a pulsed, tunable UV laser to effect dissociation of ozone. Coherent anti-Stokes Raman scattering (CARS) spectroscopy,[9] also effected with pulsed lasers, is used to record rotationally and vibrationally resolved spectra of the $O_2(^1\Delta_g)$ photofragments, before the photofragments have undergone any collisions. The experimental apparatus is represented schematically in Fig. 3.

A pulsed Nd:YAG laser (Quanta-Ray DCR-2A) serves as the "master" laser in our system. The 6 ns FWHM second harmonic output of the laser is divided into three parts. The largest part, ≈ 200 mJ, pumps a dye laser (Quanta-Ray PDL-2) whose output is used to generate the tunable UV photolysis pulse, ω_{diss}. Another part, ≈ 80 mJ, pumps a dye laser (Quanta-Ray PDL-2) whose output is used as the tunable Stokes beam, ω_s, for the CARS spectroscopy. The Stokes beam pulse energy is ≈ 8 mJ. The remaining part of the Nd:YAG second harmonic, ≈ 15 mJ, is used directly as the pump beam, ω_p, for the CARS spectroscopy. The tunable UV photolysis beam is generated by frequency doubling the dye laser output, or by mixing the frequency-doubled dye with a part of the 1.06 μm fundamental output of the Nd:YAG. The UV pulse energy is ≈ 5 mJ. The photolysis, CARS pump, and CARS Stokes beams have spectral linewidths of ≈ 0.2 cm^{-1}. The overall CARS spectral resolution, determined by the convolution of the pump and Stokes line shape functions, is ≈ 0.3 cm^{-1}. A CARS spectrum is recorded by monitoring the intensity of the anti-Stokes signal beam, $\omega_{\text{as}} = 2\omega_p - \omega_s = \omega_p + \omega_{\text{Raman}}$, as ω_s is scanned so that $\omega_p - \omega_s$ tunes through the vibrational Q-branch Raman transition frequencies, ω_{Raman}, of $O_2(^1\Delta_g)$.

The UV photolysis beam and the CARS probe beams are combined and made collinear at dichroic mirrors, and are focused into the gas cell using a 1 m focal length lens. The probe pulses are delayed with respect to the photolysis pulse

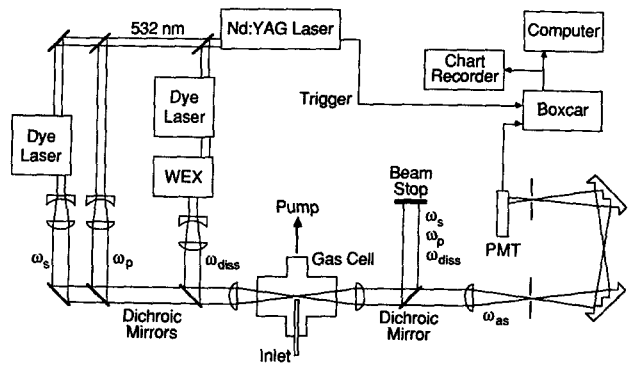

FIG. 3. Schematic diagram of the apparatus used to record CARS spectra of photofragments.

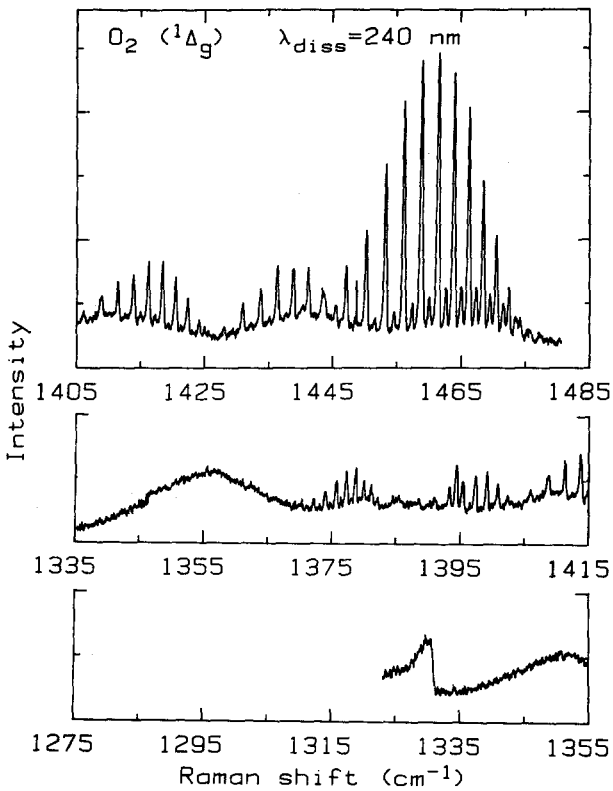

FIG. 4. Vibrational Q-branch CARS spectrum of $O_2(^1\Delta_g)$ produced by the photodissociation of O_3 at 240 nm. The $v = 0,1,2,3,4,5$, and 6 bands are at 1463, 1437, 1415, 1395, 1377, 1355, and 1328 cm^{-1}, respectively.

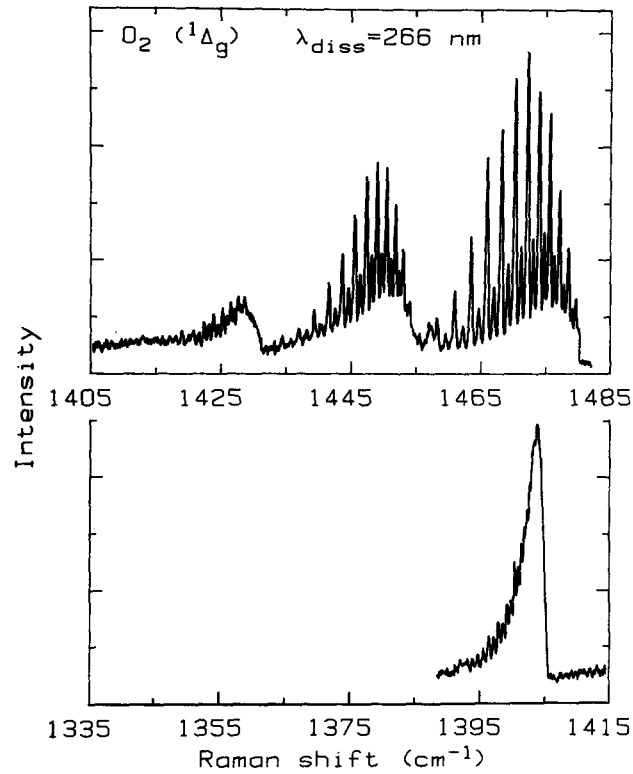

FIG. 5. Vibrational Q-branch CARS spectrum of $O_2(^1\Delta_g)$ produced by the photodissociation of O_3 at 266 nm. The $v = 0,1,2$, and 3 bands are at 1473, 1450, 1428, and 1403 cm^{-1}, respectively.

by 1 ns. Since the mean time between collisions in the gas sample ($\approx$2 Torr total pressure) is about 50 ns, the photofragments are detected under collision-free conditions and the CARS spectra reveal the nascent vibrational and rotational distributions of the $O_2(^1\Delta_g)$. After leaving the cell, the anti-Stokes signal beam is separated from the input beams by spectral and spatial filters and imaged into a photomultiplier. The output of the photomultiplier is processed by a boxcar integrator, digitized, then stored in a microcomputer for later analysis. Typically, several quick ($\approx$15 min) scans of the spectrum are taken and are averaged to produce the spectrum that is analyzed[10] to yield the photofragment quantum state populations.

Ozone for these experiments is made by ac electric discharge in pure oxygen, using a commercial ozonator. The ozone is stored on silica gel in a glass bulb at 195 K. Just prior to use any residual oxygen in the glass bulb is pumped off. During the experiments ozone is present in the gas cell at $\approx$1 Torr and flows through the cell at a rate sufficient to replenish the gas in the sampled region between laser pulses at the 10 Hz repetition rate of the Nd:YAG laser. In addition to the ozone, $\approx$1 Torr of nitrogen flows from the ends of the cell to keep the ozone localized at the center of the cell, and to ensure that the photolysis beam is not absorbed before reaching the focal region, where the CARS signal is generated.

III. RESULTS

Typical vibrational Q-branch CARS spectra of the $O_2(^1\Delta_g)$ photofragment are shown in Figs. 4–6, for photolysis of ozone at 240, 266, and 293 nm. We have obtained similar spectra at 14 other photolysis wavelengths between 230 and 311 nm. At every photolysis wavelength all energetically accessible vibrational states are populated. At 230 nm, states up to $v = 7$ are allowed, while at 311 nm, only the ground vibrational state is accessible. Thus, the spectra become much longer as the photodissociation is effected at shorter wavelengths. However, usually only a small number of the energetically allowed rotational states are produced. The range of populated rotational states within each vibra-

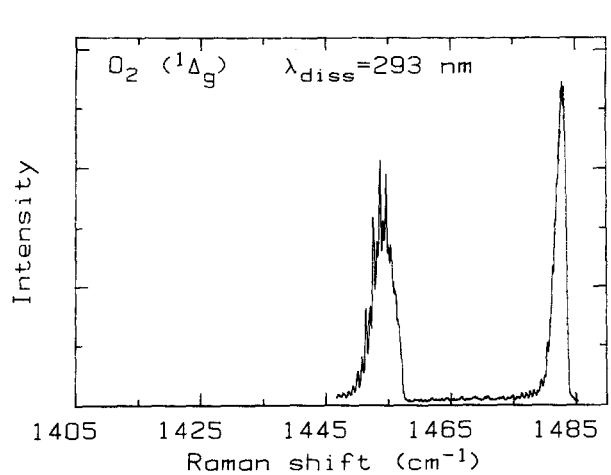

FIG. 6. Vibrational Q-branch CARS spectrum of $O_2(^1\Delta_g)$ produced by the photodissociation of O_3 at 293. nm. The $v = 0$ and 1 bands are at 1483 and 1455 cm^{-1}, respectively.

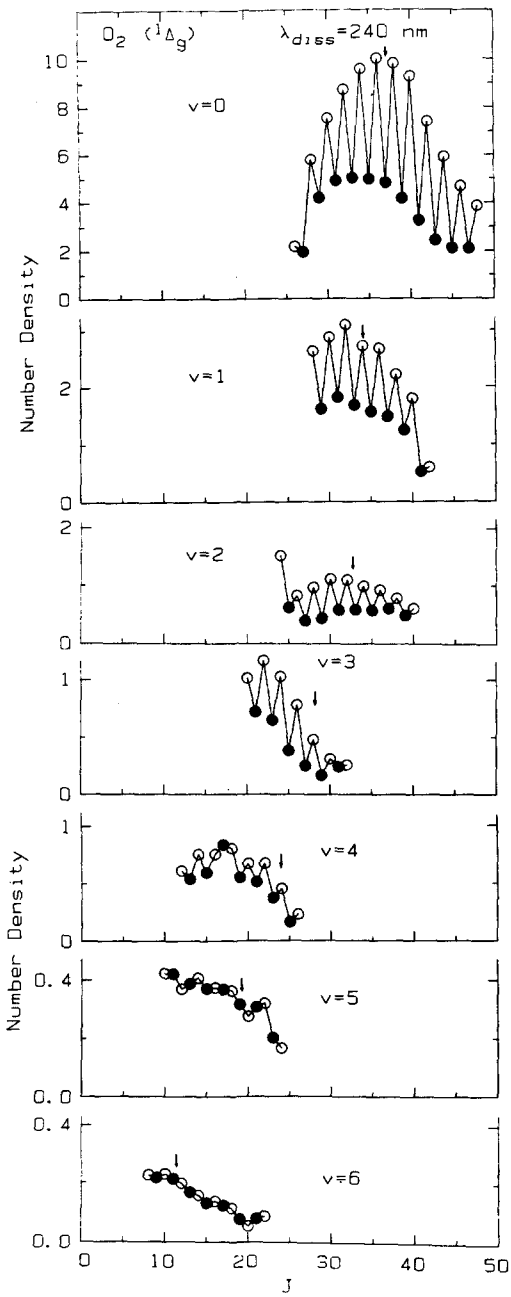

FIG. 7. Quantum state population distribution for the $O_2(^1\Delta_g)$ fragment of the 240 nm photodissociation of O_3. Even-J states are shown by open circles, odd-J states by closed circles. The arrows indicate the most probable rotational state predicted by a vibrational adiabatic, rotationally impulsive model of the dissociation dynamics.

tional state is so narrow that different vibrational bands in the spectra overlap very little, if at all. As the vibrational energy of the $^1\Delta_g$ photofragment increases, the populated rotational levels shift to lower J. As the rotational quantum number shifts to lower J, the Q-branch transitions move closer together; for $J < 12$ the spacing between lines in the Raman spectrum becomes to small to allow complete resolution of adjacent transitions at our spectral resolution (≈ 0.3 cm^{-1}).

We were not able to observe any spectra of the $O_2(^3\Sigma_g)$ photofragment at any dissociation wavelength. This is probably due to the distribution of this photofragment over thousands of rotational/vibrational states. The energy available to photofragments in the $^3\Sigma_g + {}^3P$ channel is enormous, 3.6 eV at 266 nm, and kinematic and dynamic factors promote broad state distributions for this channel. Therefore, low individual state populations are produced, and this results in very small population differences, on which the CARS signal intensity depends nonlinearly.[9]

Since the intensities in a CARS spectrum depend nonlinearly on the population difference between the quantum states connected by the Raman transition, it is not possible to read the populations directly from the spectrum. However, when the spectrum is fully rotationally resolved, analysis to extract the populations is trivial.[9,11] When the spectrum is not fully rotationally resolved, extracting the populations requires numerical analysis and we have recently developed a method to do so that is rapid, efficient, and highly accurate.[10] The methods of Ref. 10 were used here to analyze all the $O_2(^1\Delta_g)$ photofragment spectra.

One unexpected difficulty we encountered in analyzing the $O_2(^1\Delta_g)$ spectra was in assigning quantum numbers to the transitions. The spectroscopic constants[12] available for $^1\Delta_g$ were so limited in number and accuracy, that initially we were unable to assign most of the transitions we observed. The paucity of spectroscopic information available for this rather commonly encountered state of molecular oxygen is attributable to the difficulty of carrying out detailed spectroscopic measurements on a state for which transitions to all the nearby electronic states are dipole forbidden, and to the lack of a permanent dipole moment for this homonuclear diatom. Thus, in order to extract dynamical information from the line intensities, we first had to carry out a detailed spectroscopic analysis of the line positions. From this, we have been able to obtain accurate vibrational spectroscopic constants through $\omega_e z_e$, and rotational constants through γ_e, as well as an accurate internuclear potential for the $^1\Delta_g$ state of O_2. These are reported in a separate publication.[13]

Figures 7–9 show the rotational–vibrational state distributions derived from the CARS spectra of the $O_2(^1\Delta_g)$ photofragment for photolysis of ozone at 240, 266, and 293 nm. Similar state distributions have been obtained for photolysis at 14 other wavelengths in the Hartley band, between 230 and 311 nm. A test of the accuracy of the rotational/vibrational state populations derived from the CARS spectra using our analysis program,[10] is the agreement of the observed spectra with those calculated using these state populations. Figure 10 shows the typical quality of the agreement of the observed and calculated CARS spectra.

The most striking feature of all the distributions is the propensity for even-J rotational states, as we observed previously,[6] in preliminary experiments at 266 nm. This propensity is dependent on both v and J, and varies somewhat in magnitude, but is present for all vibrational states at all photolysis wavelengths. It is evident even for photolysis at 311 nm, for which the dissociation to yield $^1\Delta_g + {}^1D$ is nominally forbidden energetically and occurs only because the rotational energy of the O_3 can be tapped by the dissociation coordinate. This even-J propensity is the most surprising and most important observation of our experiments. It has

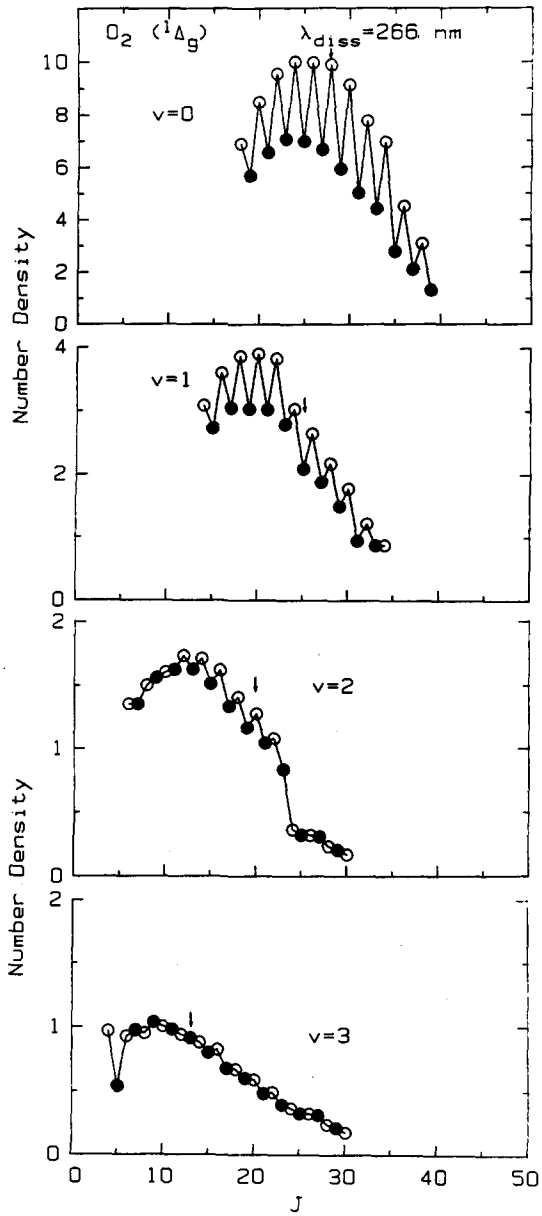

FIG. 8. Quantum state population distributions for the $O_2(^1\Delta_g)$ fragment of the 266 nm photodissociation of O_3. Even-J states are shown by open circles, odd-J states by closed circles. The arrows indicate the most probable rotational state predicted by a vibrational adiabatic, rotationally impulsive model of the dissociation dynamics.

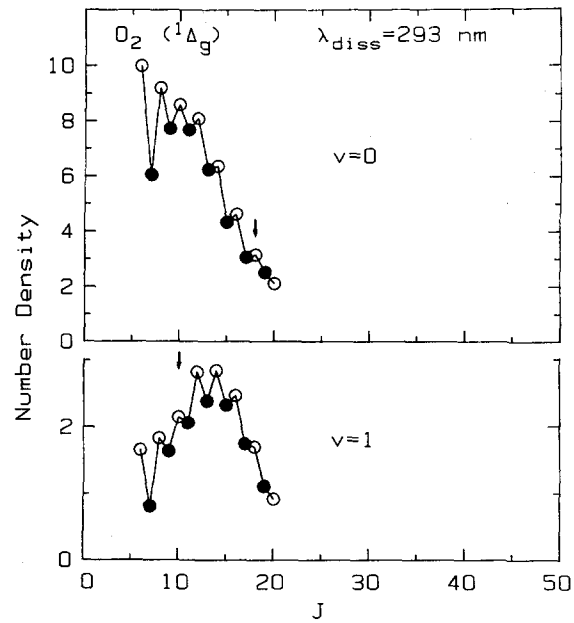

FIG. 9. Quantum state population distributions for the $O_2(^1\Delta_g)$ fragment of the 293 nm photodissociation of O_3. Even-J states are shown by open circles, odd-J states by closed circles. The arrows indicate the most probable rotational state predicted by a vibrational adiabatic, rotationally impulsive model of the dissociation dynamics.

significant and interesting implications for chemical dynamics as well as for atmospheric chemistry and cosmochemistry. The source of this even-J propensity is discussed fully in the next section.

Among the less surprising, yet still interesting, observations about the $O_2(^1\Delta_g)$ photofragment state distributions is that the rotational distribution usually peaks at quite high J. The most probable J for $v = 0$ is 36 at 240 nm and 26 at 266 nm, so the photofragments often have high rotational energy. [Note that at 300 K the most probable J for $O_2(^1\Delta_g)$ is only 8.] Despite the peaking of the rotational distribution at high J, the width of the distribution is not much greater than that for a 300 K distribution: $\Delta J_{\mathrm{FWHM}} \approx 18$ for the photofragments, compared to $\Delta J_{\mathrm{FWHM}} \approx 14$ for a thermal sample at 300 K. In Sec. IV we show that the peaking at high J is consistent with nearly impulsive rotational energy release, and that the narrow width of the distribution can be accounted for entirely by the contribution of fragment angular momentum from the thermal rotation and zero-point bending vibration of the O_3.

While at all photolysis wavelengths every energetically accessible vibrational state is observed in the photofragment state distribution, the most probable vibrational state is always this ground state. This is evident in Figs. 7–9, but can be more clearly seen in Fig. 11, in which we present the vibrational state distributions averaged over rotational state, for photolysis at five different wavelengths. Except for the opening of higher vibrational levels at shorter wavelengths, the vibrational distribution is nearly independent of photolysis wavelength, throughout the Hartley band. In Sec. IV we argue that this is evidence for the vibrational adiabaticity of the energy release; the vibrational state distribution being determined largely by Franck–Condon factors in the photoexcitation.

IV. DISCUSSION

A. Anomalous rotational distributions for $O_2(^1\Delta_g)$

The propensity for even rotational states of the $O_2(^1\Delta_g)$ photofragment at all photolysis wavelengths is intriguing. The spectra of Figs. 4–7 are of $^{16}O^{16}O$, and since ^{16}O is a spin-zero nucleus, there are no nuclear spin degeneracies to alter the relative populations of even-J and odd-J rotational states. The even-J/odd-J intensity alternation is not the result of some spectroscopic anomaly, because CARS spectra we took of $^1\Delta_g$ in a microwave discharge showed no propensity for either even- or odd-J states, just the normal CARS

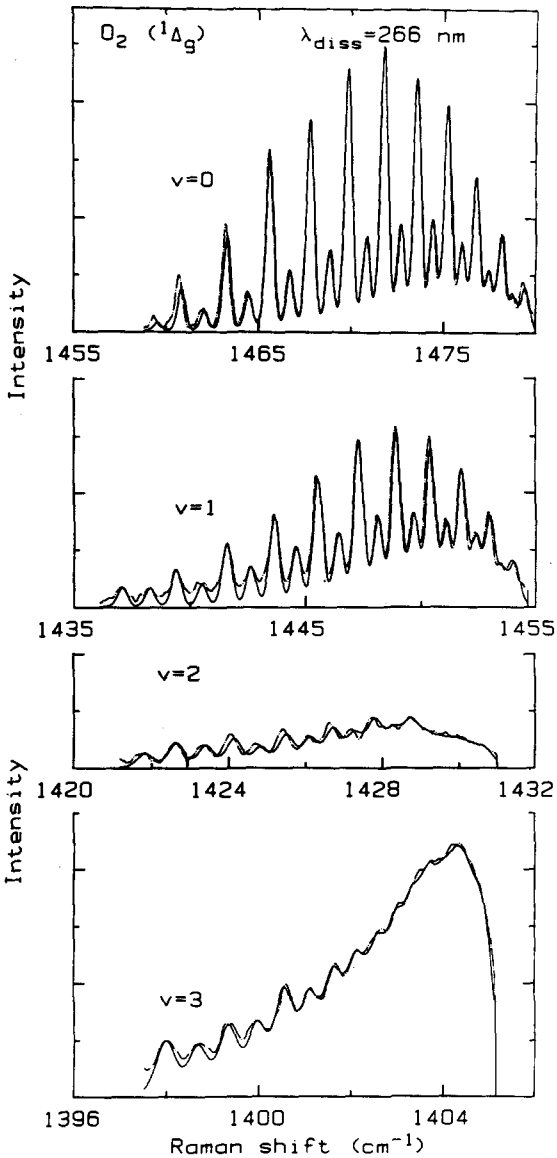

FIG. 10. Comparison of the measured vibrational Q-branch CARS spectrum for the $O_2(^1\Delta_g)$ fragment of the 266 nm photodissociation of O_3 (dot–dash line), and the spectrum calculated using the quantum state populations of Fig. 10 (solid line), see the text for explanation.

spectra expected of a near thermal rotational distribution at a somewhat elevated temperature. We thus conclude that the even-J propensity is the result of a dynamical bias in the dissociation.

As we will demonstrate below, this dynamical bias is not a selective production of even-J states of the $O_2(^1\Delta_g)$, but rather is a selective depletion of the odd-J states of $O_2(^1\Delta_g)$ by the curve crossing to the $^3\Sigma_g + {}^3P$ surface in the photolysis exit channel. This curve crossing, discussed briefly in the Introduction, is depicted in Fig. 2, which shows sections through the *ab initio* calculated[5] potential energy surfaces O_3. It is this curve crossing, not excitation to two excited states with different asymptotes, that gives the experimentally measured[2] 0.10 to 0.15 quantum yield for $O_2(^3\Sigma_g) + O(^3P)$. The odd-J selectivity of the curve crossing arises due to the selection rules that govern the crossing.

To illustrate these selection rules, we describe the curve crossing in a simple diabatic representation. While the curve crossing is formally an avoided crossing, since all the surfaces involved are of A' symmetry in the C_s group representing the O_3 molecule when the two bond lengths are no longer equivalent, a description in the diabatic representation is more convenient here, as it often is when discussing collisional curve crossings.[14] In a diabatic representation the curve crossing between the initially prepared state, "B" in Fig. 2, and the "destination" state "R" in Fig. 2, is induced by the off-diagonal matrix element, $|\langle\Phi_R|H_{el}|\Phi_B\rangle|^2$, where Φ_R and Φ_B are the wave functions on the diabatic surfaces, and are not eigenfunctions of the electronic Hamiltonian H_{el}. In the diabatic representation the Born–Oppenheimer approximation is still valid, so this matrix element can be written as a product of an electronic part and several nuclear parts, $|\langle\Phi_R|H_{el}|\Phi_B\rangle = |\langle\Phi_{R,el}|H_{el}|\Phi_{B,el}\rangle \times \langle\Phi_{R,vib}|\Phi_{B,vib}\rangle \times \langle\Phi_{R,rot}|\Phi_{B,rot}\rangle \times \langle\Phi_{R,trans}|\Phi_{B,trans}\rangle$. Here we have used an atom–diatom basis for the nuclear coordinates, so the vibrational functions and the rotational functions are those for O_2, and the translational function describes the O–O_2 relative motion. An atom–diatom basis is appropriate because the curve crossing occurs at large O–O_2 separation, for which the interaction energy on the B surface is negligible, as shown in Fig. 2.

Selection rules governing the curve crossing arise in part due to symmetry or parity constraints on the nuclear part of the matrix element above. Of particular importance is the rotational overlap integral, $\langle\Phi_{R,rot}|\Phi_{B,rot}\rangle$. This integral is zero unless the rotational functions are of identical parity. Since the rotational functions are of even parity if J is even, and odd parity if J is odd, the parity of the wave functions introduces the selection rule $\Delta J = 0, \pm 2, \pm 4, \pm 6, \ldots$[15] This selection rule would be of little consequence were it not for the fact that $^{16}O^{16}O$ in the ground $^3\Sigma_g$ state (as a $^3\Sigma_g^-$ state) has only odd-J rotational states, due to the restriction that the overall wave function be even with respect to exchange of the spin-zero ^{16}O nuclei.[16] Since the rotational function $\Phi_{R,rot}$ has only odd-J states, the $\Delta J = 0, \pm 2, \pm 4, \pm 6, \ldots$ selection rule implies that the crossing from B to R, that is from $^1\Delta_g + {}^1D$ to $^3\Sigma_g + {}^3P$, is allowed only for $O_2(^1\Delta_g)$ in

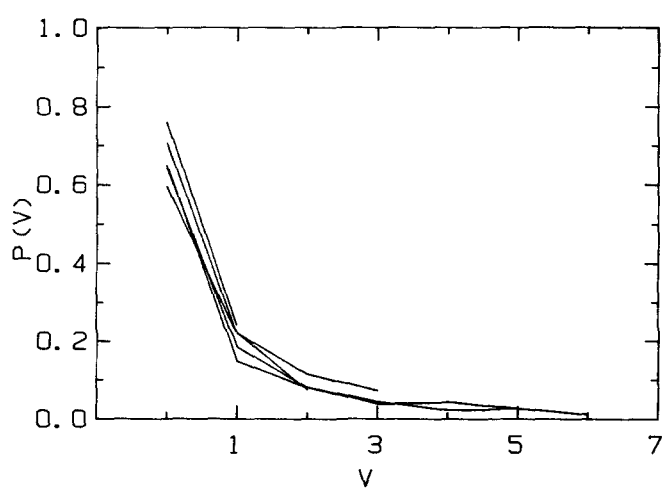

FIG. 11. Vibrational state distribution for $O_2(^1\Delta_g)$ from the photodissociation of O_3 at 240, 248, 266, 280, and 293 nm.

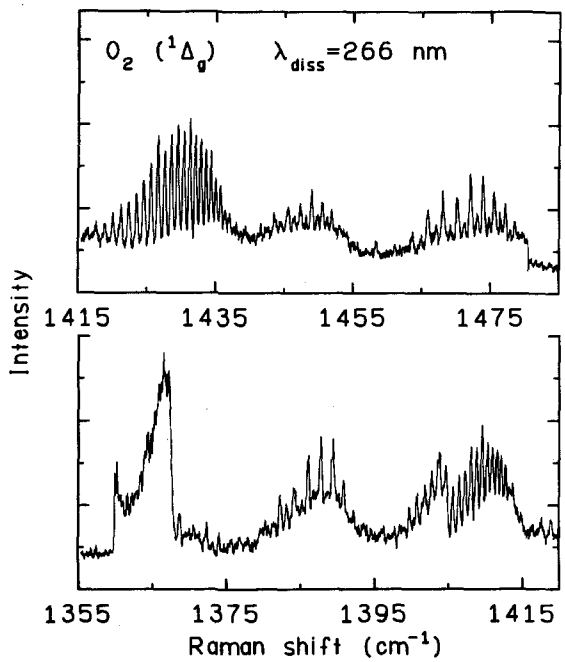

FIG. 12. Part of the vibrational Q-branch CARS spectrum of $O_2(^1\Delta_g)$ produced by the 266 nm photodissociation of ^{18}O enriched O_3 containing ^{16}O and ^{18}O in a 1:1 ratio. Among the bands shown in this part of the spectrum are the $v=0$ and $v=1$ bands of $^{16}O^{16}O$ at 1474 and 1448 cm^{-1}, the $v=0$ and $v=1$ bands of $^{16}O^{18}O$ at 1430 and 1410 cm^{-1}, and the $v=0$ band of $^{18}O^{18}O$ at 1388 cm^{-1}.

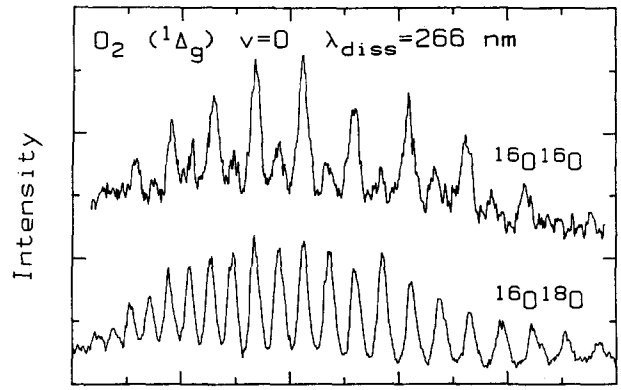

FIG. 13. Expanded scale plots of the $v=0$ bands of the vibrational Q-branch CARS spectra of $^{16}O^{16}O$ and $^{18}O^{16}O$ photofragments produced by the 266 nm photodissociation of a 1:1 ^{18}O:^{16}O O_3 sample, taken from Fig. 5. The spectra have been both shifted and scaled along the horizontal (Raman shift) axis so that peaks of the same J lie directly above/below one another.

odd-J rotational states. Thus, the effect of the curve crossing on the $^1\Delta_g$ state is to deplete selectively the odd-J rotational states, while leaving unaffected the even-J rotational states.

If this explanation is correct, the difference between the even-J state populations and the odd-J populations of $^1\Delta_g$ is an indirect measure of the $^3\Sigma_g + {}^3P$ quantum yield, and should agree with direct measurements of the quantum yield. Indeed, we find such agreement. Upon summing the $^1\Delta_g$ quantum state populations over v and J for even-J states only, and over v and J for odd-J states only, and then comparing these sums, we find an implied $^3\Sigma_g + {}^3P$ quantum yield at 266 nm of 0.15 ± 0.03, in agreement with the 0.12 ± 0.02 value reported by Brock and Watson[17] based on direct resonance fluorescence measurements at this wavelength, and in agreement with the ≈ 0.1 value at 266 nm derived from the molecular beam experiments of Sparks *et al.*[16]

Such agreement, while encouraging, could be fortuitous. To prove the curve crossing hypothesis, we need to alter the experimental conditions so as to produce in the even-J/odd-J population ratio a change that is consistent only with the curve crossing hypothesis. The use of isotopically heterogeneous O_3 in the photodissociation experiments provides the opportunity to do so.

The curve crossing is parity-restricted to odd-J rotational states of $^1\Delta_g$ only because the $^3\Sigma_g$ state for homonuclear $^{16}O^{16}O$ has only odd-J states, due to the requirement that the overall wave function be even with respect to exchange of the spin-zero ^{16}O nuclei. For heteronuclear $^{18}O^{16}O$ or $^{17}O^{16}O$, the overall wave function has no symmetry with respect to exchange of the nonidentical nuclei, and so for these species there are both even-J and odd-J rotational levels in the $^3\Sigma_g$ electronic state. The existence of both even and odd O_2 rotational states in the $^3\Sigma_g$ state will make curve crossing from $^1\Delta_g$ to $^3\Sigma_g$ allowed for both odd-J and even-J states of $^1\Delta_g$, and the propensity for even-J rotational states for $^1\Delta_g$ will disappear.

To test this prediction, we have carried out CARS photofragment spectroscopy on $O_2(^1\Delta_g)$ formed in the photodissociation of isotopically heterogeneous ozone, containing ^{16}O and ^{18}O in a 1:1 ratio. The ozone was made by electric discharge, from O_2 feedstock containing equal amounts of $^{16}O^{16}O$ and $^{18}O^{18}O$. CARS spectroscopy of this isotopically mixed ozone showed that it contained all possible O_3 isotopomers, in the statistically expected amounts. Upon photodissociation of this ozone at 266 nm we recorded the CARS spectrum shown in Fig. 12.

Due to the appreciable isotope shifts in the Raman spectrum, and the narrow rotational state distribution in each vibrational level, we can observe and identify in Fig. 12 transitions due to $^{16}O^{16}O$, $^{16}O^{18}O$, and $^{18}O^{18}O$. The $v=0$ and $v=1$ bands of $^{16}O^{16}O$ are clearly evident at 1474 and 1448 cm^{-1}, and these bands show the same intensity pattern, in particular the even-J propensity, we observe upon 266 nm photodissociation of pure ^{16}O ozone (Fig. 5). The $v=0$ and $v=1$ bands of $^{16}O^{18}O$ are at 1430 and 1410 cm^{-1}, and as predicted by the curve crossing hypothesis, they show no propensity for even-J or odd-J rotational states. Also as expected, the $v=0$ band of the zero nuclear spin $^{18}O^{18}O$ homonuclear species, at 1388 cm^{-1}, which is superimposed on the rotationally unresolved $v=2$ band of $^{16}O^{18}O$, shows the same propensity for even-J rotational states that the homonuclear $^{16}O^{16}O$ species displays. The differences between the $^{16}O^{18}O$ ($^1\Delta_g$) spectra and the $^{16}O^{16}O$ ($^1\Delta_g$) spectra are most clearly shown in Fig. 13, where we plot the $v=0$ bands of these two species together, shifted and scaled so that transitions from identical J lie directly above/below one another.

The qualitative difference of Fig. 13 between the homonuclear $^{16}O^{16}O$ and heteronuclear $^{16}O^{18}O$ in even-J/odd-J behavior is necessary, but not sufficient, evidence to prove

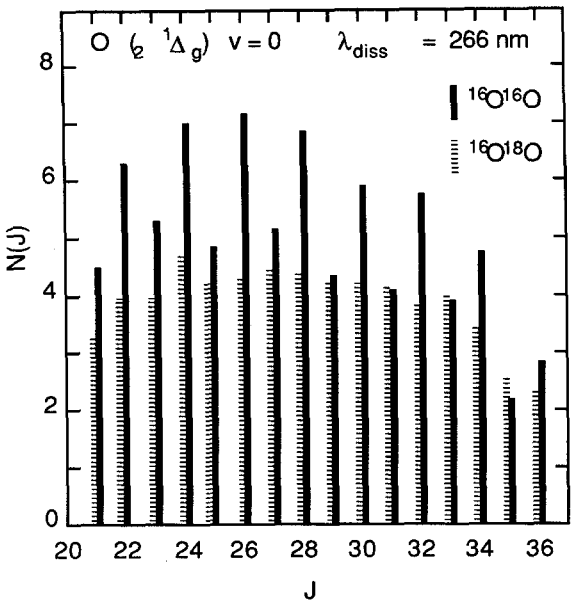

FIG. 14. Quantum state population distributions for the $^{16}O^{16}O$ and $^{18}O^{16}O$ photofragments produced by the 266 nm photodissociation of a 1:1 ^{18}O:^{16}O O_3 sample. The populations have been corrected for the two times greater statistical abundance of the heteronuclear species.

the curve crossing hypothesis. To prove this hypothesis, we must demonstrate that the difference between $^{16}O^{16}O$ $^1\Delta_g$ and $^{16}O^{18}O$ $^1\Delta_g$ is that in the latter, the curve crossing depletes both even-J and odd-J states equally. That is, we must show that relative to $^{16}O^{16}O$ $^1\Delta_g$ the even-J rotational states of $^{16}O^{18}O$ $^1\Delta_g$ have a reduction in population, while the odd-J states of $^{16}O^{16}O$ $^1\Delta_g$ and $^{16}O^{18}O$ $^1\Delta_g$ have equal populations.

The CARS spectrum of Fig. 12 shows that this is precisely the difference between the homonuclear and heteronuclear $^1\Delta_g$ diatomic fragment populations. Figure 14 presents a plot of the rotational population distribution in $v = 0$ for $^{16}O^{16}O$ $^1\Delta_g$ and $^{16}O^{18}O$ $^1\Delta_g$, corrected for the relative abundances of the two O_2 isotopomers. The odd-J populations are almost identical (the $^{16}O^{18}O$ populations are on average $90 \pm 6\%$ of the $^{16}O^{16}O$ populations), while the even-J populations of $^{16}O^{18}O$ $^1\Delta_g$ are $68 \pm 5\%$ of the $^{16}O^{16}O$ $^1\Delta_g$ even-J populations. This is almost exactly the same as the average odd-J-to-even-J population percentage in $^{16}O^{16}O$ $^1\Delta_g$ $v = 0,74 \pm 5\%$. In $^{16}O^{18}O$ the odd-J population is on average $99 \pm 5\%$ of the even-J population. Summed over all v and J, the total population of $^1\Delta_g$ $^{16}O^{18}O$ is only $\approx 75\%$ of the total population of $^1\Delta_g$ $^{16}O^{16}O$, that is the quantum yield for $^1\Delta_g$ is smaller when $^{16}O^{18}O$ is produced than when $^{16}O^{16}O$ is formed. Each of these observations is, within experimental uncertainty, in exact quantitative agreement with the predictions of the curve-crossing hypothesis.

A direct, quantitative comparison of the state populations for the $^{16}O^{16}O$ and $^{16}O^{18}O$ fragments in photodissociation of the ^{18}O enriched ozone sample is possible, because we know the relative probabilities of forming $^{16}O^{16}O$ and $^{16}O^{18}O$, from our knowledge of the relative abundances of all the O_3 isotopomers. Because of the statistical distribution of isotopomers in this 1:1 ^{16}O:^{18}O mixture, the probability of forming $^{16}O^{18}O$ is twice as great as the probability of forming $^{16}O^{16}O$. This is why the $^{16}O^{18}O$ peaks in Fig. 12 are more intense than the $^{16}O^{16}O$ peaks, even though the quantum yield for $^1\Delta_g$ is smaller for the heteronuclear species. In preparing Fig. 14, all the $^{16}O^{18}O$ populations extracted from the CARS spectrum were divided by 2 to correct for the greater probability of forming the heteronuclear fragment.

These results also clearly show that there is no contribution to the population difference between even-J and odd-J rotational states from a propensity for the Δ^+ Λ-doublet component of $^1\Delta_g$. Preferences for a particular Λ-doublet component of the photodissociation fragments have been observed before.[19] In $O_2(^1\Delta_g)$ a Λ-doublet preference would have an unusual consequence. The Δ^+ component has only the even-J rotational states of $^1\Delta_g$, while the Δ^- component has only the odd-J rotational states of $^1\Delta_g$, because of the same nuclear exchange symmetry restrictions that allow only odd-J states in $^{16}O^{16}O$ $^3\Sigma_g$.[16] Thus, if there were a propensity for the Δ^+ component of O_2 in ozone photodissociation, there also would be, coincidentally, a preference for even-J rotational states.

If a Λ-doublet propensity were the factor governing the even-J/odd-J population difference, this difference would disappear for heteronuclear $^{16}O^{18}O$ $^1\Delta_g$ fragments, for which there are both even-J and odd-J rotational states for both Λ-doublet components. Although the Λ-doublet propensity itself would not be affected, this propensity would not produce any J propensity. However, the quantitative way in which the even-J and odd-J populations for $^{16}O^{18}O$ would change relative to those for $^{16}O^{16}O$ is quite different from the changes we actually observe. The odd-J rotational state populations of $^{16}O^{18}O$ would be 118% of the odd-J state populations for $^{16}O^{16}O$, while the even-J $^{16}O^{18}O$ populations would be 87% of the corresponding $^{16}O^{16}O$ populations. Moreover, the $^1\Delta_g$ populations summed over all rotational and vibrational states would be exactly the same for $^{16}O^{16}O$ and $^{16}O^{18}O$, since the only difference between the two would be a different distribution among the rotational states of $O_2(^1\Delta_g)$.

These experiments with isotopically mixed ozone not only prove the curve crossing explanation for the odd-J/even-J anomaly in $O_2(^1\Delta_g)$, they also illustrate the most important consequence of the curve crossing selection rules: the curve crossing is isotopically selective. Since for the $^{16}O^{18}O$ photofragment curve crossing from both odd-J and even-J rotational states of $^1\Delta_g$ is allowed, the quantum yield for $^3\Sigma_g$ for this species is twice as great as that for the $^{16}O^{16}O$ species. The same is true for the $^{16}O^{17}O$ diatom relative to $^{16}O^{16}O$. Therefore, in the photodissociation of naturally occurring O_3, for which the ^{18}O and ^{17}O abundances are quite low, the $^3\Sigma_g$ product becomes enriched in ^{18}O and ^{17}O, while the $^1\Delta_g$ product becomes depleted of these isotopes. This happens because the probability of forming $^{18}O^{18}O$ or $^{17}O^{17}O$ is very, very small; when the rare isotopes are present it will be as $^{18}O^{16}O$ and $^{17}O^{16}O$, for which the $^3\Sigma_g$ yield is higher than for the abundant $^{16}O^{16}O$ homonuclear species.

The doubling of the $^3\Sigma_g$ quantum yield for the heteronuclear diatoms makes the ^{18}O and ^{17}O isotopic enrichment of

TABLE I. Quantum yield for $^3\Sigma_g + {}^3P$ in O_3 photodissociation.

Wavelength, nm	$O_2(^3\Sigma_g) + O(^3P)$ quantum yield[a]
266	0.15(± 0.03)[b]
280	0.08
291	0.11
293	0.14
300	0.06
305	0.10
309	0.12
311	0.11

[a] Calculated assuming that the photodissociation quantum yield is unity, and that the only dissociation channels are $O_2(^3\Sigma_g) + O(^3P)$ and $O_2(^1\Delta_g) + O(^1D)$. See the text for details.

[b] Uncertainty for all values.

$^3\Sigma_g$ and depletion of $^1\Delta_g$ very large. This isotopic fractionation has significant implications for atmospheric ozone photochemistry, and for cosmochemical uses of oxygen isotopic ratio measurements. These are discussed in the following article.[7] We mention here only the unique feature of the isotopic fractionation: it is independent of isotopic mass, giving equal enrichment/depletion of ^{18}O and ^{17}O. This kind of mass-independent isotopic fractionation will not be limited to curve crossing in photodissociation or to oxygen isotopes. Any linear molecule, containing symmetrically located atoms for which the commonly occurring isotope is a spin-zero nucleus, will display mass-independent isotopic fractionation in the curve crossing from a Π or Δ electronic state to a Σ electronic state, leading to enrichment of the Σ state and depletion of the Π or Δ state in the rare isotopes.[7] For the isotopically mixed species, the curve crossing rate is twice as great as for the homonuclear common isotope species, due to twice as many Π or Δ rotational states being allowed to cross. In a simple but elegant series of experiments, Thiemens and co-workers have measured equal $^{17}O,^{18}O$ isotopic fractionation in oxygen-containing samples subjected to electric discharge.[20] The kind of mass-independent isotopic fractionation described here may be the source of the effects they have observed.[7]

Since it is the curve crossing to $^3\Sigma_g + {}^3P$ that causes the depletion of the $^1\Delta_g$ odd-J states, we can use our CARS spectra of $^1\Delta_g$ to determine indirectly the quantum yield of the triplet products, simply by summing the individual state populations over all even-J and all v, and separately summing over all odd-J and all v, then comparing the sums. The quotient $(\Sigma_{\text{even-}J} - \Sigma_{\text{odd-}J})/(2\Sigma_{\text{even-}J})$ gives the triplet yield, if we assume that the total photodissociation yield is unity and that the only product channels are $^1\Delta_g + {}^1D$ and $^3\Sigma_g + {}^3P$. This implied quantum yield is given in Table I for eight of the wavelengths studied here.

Although we have recorded CARS spectra of $^1\Delta_g$ produced at shorter wavelengths, we cannot as confidently extract the $^3\Sigma_g + {}^3P$ quantum yields from them as we can for the spectra at the wavelengths listed in Table I. At photolysis wavelengths shorter than 266 nm, we may have some small contribution to the even-J/odd-J population difference from selective populations of even-J states due to the preferential production of the Δ^+ Λ doublet discussed above. At shorter photodissociation wavelengths, the fragment shifts to higher J. Since a Λ-doublet propensity will increase rapidly with increasing J,[19] our demonstration, using $^{16}O^{18}O$, that there is no Λ-doublet propensity at 266 nm does not prove its *complete* absence at shorter wavelengths. We have not carried out any experiments with ^{18}O enriched ozone at these shorter wavelengths, and such experiments give the only unequivocal means of separating the curve crossing and Λ-doublet effects.

Over the range 266 to 311 nm, the average value of the $^3\Sigma_g + {}^3P$ quantum yield is 0.11. The fluctuation in the yield from 266 to 311 nm is not statistically significant, because the accuracy of our measurements is only ± 0.03. Thus, our spectra of $O_2(^1\Delta_g)$ indicate that the $^1\Delta_g + {}^1D/{}^3\Sigma_g + {}^3P$ branching ratio is 0.89/0.11, independent of wavelength, right up to and slightly beyond the nominal thermodynamic threshold for the singlet channel, 310 nm. This is in agreement with other results, except at $\lambda > 308$ nm, for which other measurements of the $O(^1D)$ production show a declining quantum yield for increasing wavelength, and an $O(^1D)$ yield of only 0.35 at 311 nm.[2,21] This disagreement can be explained if one of the assumptions we invoke in order to obtain quantum yields from our $O_2(^1\Delta_g)$ measurements is not true, that is, if the quantum yield for dissociation is less than unity for $\lambda > 308$ nm, or if there is another dissociation channel in addition to $^1\Delta_g + {}^1D$ and $^3\Sigma_g + {}^3P$.

It seems unlikely that the net dissociation quantum yield could be less than unity at these wavelengths[21,22] and it would have to be considerably less than unity. Using our measurements of the relative yields of the $^1\Delta_g + {}^1D$ and $^3\Sigma_g + {}^3P$ channels, and the $O(^1D)$ absolute quantum yield measurements of Brock and Watson,[1,21] the implied net dissociation quantum yield would be only 0.82, 0.70, 0.53, and 0.40 at 308, 309, 310, and 311 nm, respectively.

It seems more likely that there is an additional dissociation channel at the long wavelength end of the Hartley absorption band. It is known that the photodissociation of O_3 at 334 nm proceeds by a spin-forbidden process yielding $O(^3P) + O_2(^1\Delta_g)$ or $O_2(^1\Sigma_g)$,[23] and this channel may make some contribution at 308–311 nm as well. Our O_2 CARS spectra show no evidence for the appearance of an $O(^3P) + O_2(^1\Delta_g)$ channel as the photolysis is effected at longer wavelengths, which would be expected to be accompanied by a change in the rotational and vibrational state distributions of the $O_2(^1\Delta_g)$. When photolyzing O_3 at long wavelengths we did not look for $O_2(^1\Sigma_g)$, which has a Raman spectrum beginning at 1405 cm^{-1} and extending to smaller Raman shifts, so we cannot comment on its possible formation. In order to reconcile our relative $^1\Delta_g + {}^1D$ and $^3\Sigma_g + {}^3P$ yields, and the $O(^1D)$ absolute quantum yield measurements of Brock and Watson,[1,21] the quantum yield of an $O(^3P) + O_2(^1\Sigma_g)$ channel would have to be appreciable, about 0.56 at 311 nm, for example.

B. Photodissociation dynamics

Other than the propensity for even-J rotational states, the two dominant features of the $O_2(^1\Delta_g)$ photofragment state distributions are the narrow rotational distributions,

usually peaking at high J, and the relative insensitivity of the vibrational state distribution to variation of the photolysis wavelength. These dynamical characteristics are very similar to those displayed by the quantum state distributions of $O_2(^3\Sigma_g)$ produced in the visible (532–638 nm) photolysis of ozone.[11,24] In the visible photolysis, we observed that the O_2 vibrational distribution was almost completely independent of photolysis wavelength, while the rotational distribution was always peaked at high J and always had the same narrow width. We showed that this was exactly the behavior expected for dissociation dynamics that are vibrationally adiabatic, but rotationally impulsive, and that this simple model could quantitatively account for all aspects of the photofragment state distribution. This interpretation is not as clear-cut for the UV photodissociation, since the rotational and vibrational distributions do change somewhat with wavelength. However, rotationally impulsive, vibrationally adiabatic energy release must still dominate the dissociation dynamics.

For rotationally impulsive, but vibrationally adiabatic energy release in the photofragmentation, conservation of energy and momentum dictate a unique final rotational state for each fragment vibrational state, if we neglect the contributions to the $O_2(^1\Delta_g)$ fragment angular momentum from the O_3 rotation and bending vibration.[8,11,24] The final state expected is determined by the O_3 ground electronic state bond angle and the available energy, the total energy minus the O_2 fragment vibrational energy. The O_2 rotational states predicted by this model are indicated by the arrows in the photofragment state distributions of Figs. 7–9. The O_2 rotational state predicted by the model is usually in reasonable agreement with the observed most probable rotational state. However, when one includes the O_3 rotation and bending vibration in the rotationally impulsive model calculation, there are clear differences between the model predictions and the observations: the observed distribution always peaks at lower J than the model distribution.[8] This indicates that energy release is not perfectly impulsive, even rotationally.

Even though the peak of the rotational distributions calculated using the rotationally impulsive model is incorrect, the width of the calculated distributions exactly reproduces the width and shape of the observed distributions, but only if we restrict the calculation to reflect a vector correlation of the different sources of O_2 fragment angular momentum.[8] The vector correlation operative here is that the O_2 fragment rotational angular momentum derived from the in-plane rotation of the O_3 must be parallel to the O_2 angular momentum induced by the dissociative impulsive energy release.

The vector correlation is such as to exclude the fragment state of higher orbital angular momentum/recoil linear momentum when two energy and total angular momentum degenerate fragment states are available. The two degenerate states correspond to breaking of one or the other of the two equivalent bonds in these C_{2v} molecules. The angular momentum associated with the in-plane rotation of the parent molecule lifts the "degeneracy" of the two otherwise equivalent bonds, because as a result of this angular momentum the fragment rotational and orbital angular momenta and recoil linear momenta depend on which bond is broken. Dissociation occurs by the scission of whichever of the two equivalent bonds leads to minimum orbital angular momentum/recoil linear momentum. The fragment state of least orbital angular momentum/recoil linear momentum gives much larger Franck–Condon overlap between the initial bound state and the final continuum state in the photoexcitation, and this may be the source of the bond "selectivity" in the dissociation.[8]

That the dynamics of the UV dissociation of ozone are close to being vibrationally adiabatic is no more surprising than the even closer approximation to vibrational adiabaticity in the visible photodissociation of ozone.[11,23] Ozone has a rather small bond angle in the ground state, 116.8°,[26,26] and *ab initio* structure calculations[5] indicate that the equilibration bond angle in the $^1B_2$ state prepared by the UV excitation is not much different, 108°. Because of this small bond angle, even very impulsive energy release in the dissociation will not be effective in exciting the O_2 vibrationally, because the projection of the impulses along the O_2 bond will be very small.

Vibrational excitation could still result however, if the bond lengths in the $^1A_1$ and $^1B_2$ states of ozone differed significantly, or if the bond length in $O_2(^1\Delta_g)$ were significantly different from that in O_3. The equilibrium bond length in the ground $^1A_1$ electronic state of ozone is 1.271 Å,[25] not much different from that of oxygen in the $^1\Delta_g$ state, 1.215 Å,[12] but *ab initio* calculations[5] give 1.405 Å for the equilibrium bond length in the excited $^1B_2$ state of ozone. On the basis of these bond lengths, we expect that the Franck–Condon vibrational overlaps in the photoexcitation, which are overlaps between $O_2(^1\Delta_g) + O(^1D)$ and $O_3(^1A_1)$, will give high probability only to the formation of the ground vibrational state of the O_2 photofragment, since the equilibrium bond length in $O_3(^1A_1)$ lies within the ground vibrational state zero-point motion of $O_2(^1\Delta_g)$.[12] However, we can expect some elongation of the preserved O_3 bond during the separation of the photofragments, due to the larger equilibrium bond length in the dissociative $^1B_2$ state, and some concomitant probability of formation of excited states of the diatomic fragment. Nonetheless, the populations of the excited vibrational states should be much smaller than the population of the ground state. The O–O bond elongation is driven by the projection of the potential energy surface gradient along the direction of the preserved bond, and this gradient is likely to be large only in the Franck–Condon region, since the initial $O_3(^1A_1)$, and final $O_2(^1\Delta_g)$, bond lengths are so similar. The projection of the potential energy surface gradient along the dissociating bond drives the system out of the Franck–Condon region very quickly, and there is likely to be little time for the gradient along the preserved bond to act.

The predominant formation of the ground vibrational state of the diatomic fragment at all wavelengths in the UV dissociation of O_3, as shown in Fig. 11, is at least qualitatively in agreement with this picture of the dissociation dynamics. We note here that the vibrational state distributions we measure directly are corroborated by vibrational distributions derived from the molecular beam photofragment velocity distributions of Sparks *et al.*[18] as indicated in Fig. 15. The small differences in the two distributions are probably due to uncertainties in the deconvolution of the velocity dis-

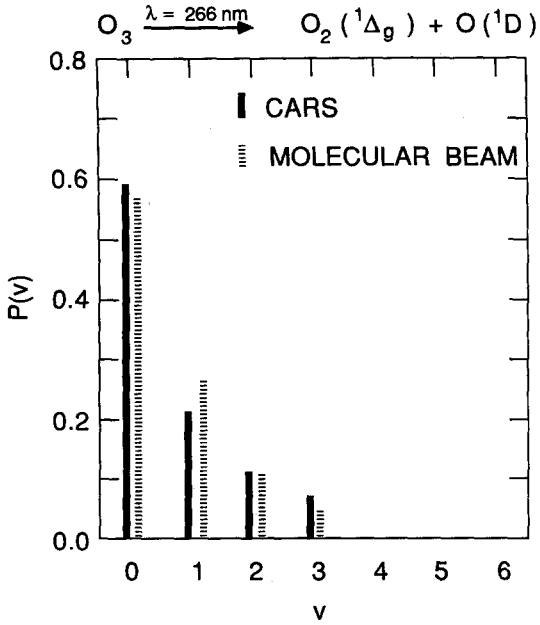

FIG. 15. Comparison of the vibrational state distributions for the $O_2(^1\Delta_g)$ photofragment from the 266 nm photodissociation of O_3 derived from molecular beam photofragment translational spectroscopy, Ref. 18, and those measured directly by CARS spectroscopy, present work.

tributions, for which the velocity resolution was not sufficient to separate completely contributions from fragments in different vibrational states.

The predominant formation of the ground vibrational state of the $O_2(^1\Delta_g)$ fragment in the UV dissociation of O_3 implies that the fragments are formed with large translational energy when the dissociation is effected at wavelengths appreciably shorter than the thermodynamic threshold wavelength, 310 nm. Even though high-J $O_2(^1\Delta_g)$ rotational states are produced, angular momentum constraints preclude a large fraction of the available energy from

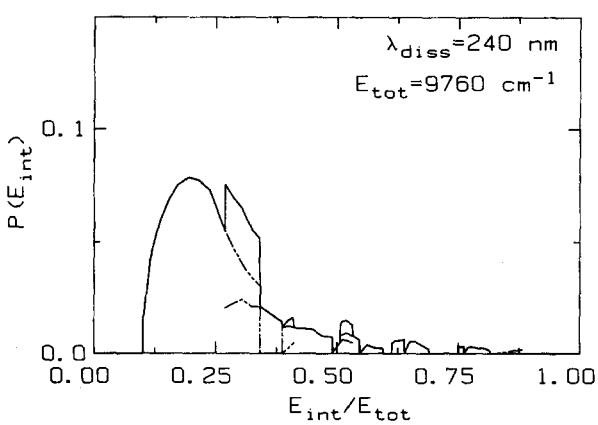

FIG. 16. Internal energy (rotation plus vibration) distribution for the $O_2(^1\Delta_g)$ photofragment from the 240 nm photodissociation of ozone. The total energy is given by the photon energy minus the bond dissociation energy of ozone (1.05 eV, Ref. 27), minus the electronic energy of the $O_2(^1\Delta_g)$ and $O(^1D)$ states (0.977 and 1.967 eV, Ref. 22), plus the average rotational energy of the O_3 (0.039 eV). The dashed lines give the contributions from individual vibrational states, while the solid line is a sum over all vibrational states.

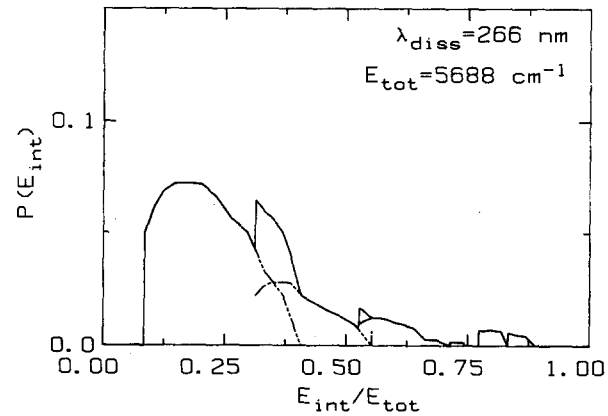

FIG. 17. Internal energy (rotation plus vibration) distribution for the $O_2(^1\Delta_g)$ photofragment from the 266 nm photodissociation of ozone. The total energy is given by the photon energy minus the bond dissociation energy of ozone (1.05 eV, Ref. 27), minus the electronic energy of the $O_2(^1\Delta_g)$ and $O(^1D)$ states (0.977 and 1.967 eV, Ref. 22), plus the average rotational energy of the O_3 (0.039 eV). The dashed lines give the contributions from individual vibrational states, while the solid line is a sum over all vibrational states.

appearing as fragment rotation. The $O_2(^1\Delta_g) + O(^1D)$ internal energy distributions of Figs. 16–18 illustrate this very clearly. The fragment internal energy distributions are peaked at such low energies that more than 75% of the available energy is in $O + O_2$ translation. At 240 nm, the $O(^1D)$ fragment has a most probable translational energy of nearly 0.7 eV.

V. CONCLUSION

Vibrationally and rotationally resolved CARS spectra of the $O_2(^1\Delta_g)$ photofragment have been obtained for photolysis of O_3 at 17 wavelengths throughout the Hartley band. These spectra reveal an apparent propensity for the formation of even-J rotational states of this fragment. Our experi-

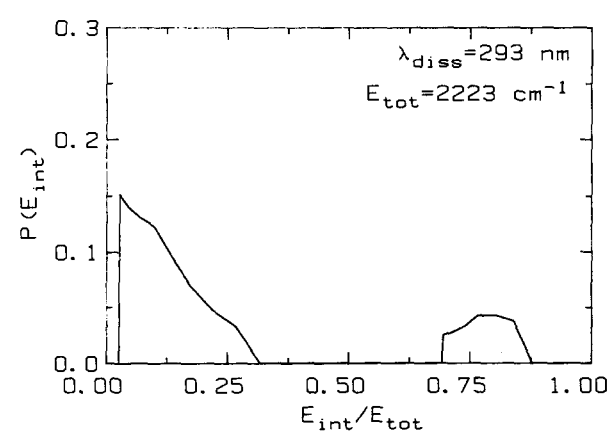

FIG. 18. Internal energy (rotation plus vibration) distribution for the $O_2(^1\Delta_g)$ photofragment from the 293 nm photodissociation of ozone. The total energy is given by the photon energy minus the bond dissociation energy of ozone (1.05 eV, Ref. 27), minus the electronic energy of the $O_2(^1\Delta_g)$ and $O(^1D)$ states (0.977 and 1.967 eV, Ref. 22), plus the average rotational energy of the O_3 (0.039 eV).

ments show that this effect actually is a selective depletion of odd-J rotational states of $O_2(^1\Delta_g)$ by a curve crossing from $O_2(^1\Delta_g) + O(^1D)$ to $O_2(^3\Sigma_g) + O(^3P)$. The odd-J depletion selectivity occurs only for $^{16}O^{16}O$ oxygen, not for $^{17}O^{16}O$ or $^{18}O^{16}O$ oxygen. For the heteronuclear species the curve crossing depletes both even-J and odd-J states equally. This behavior results from the restriction that the rotational wave function parity remain unchanged upon curve crossing, coupled with the presence of even-J rotational states for $^{17}O^{16}O$ and $^{18}O^{16}O(^3\Sigma_g)$ and their absence for $^{16}O^{16}O(^3\Sigma_g)$. Because of this, the curve crossing is isotopically selective, the quantum yield of $O_2(^3\Sigma_g)$ is twice as great for $^{18}O^{16}O$ and $^{17}O^{16}O$ as it is for $^{16}O^{16}O$, and dissociation of ozone leads to mass-independent isotopic fractionation.

Analysis of the CARS spectra of $O_2(^1\Delta_g)$ also reveals that the UV dissociation dynamics of ozone are largely vibrationally adiabatic, but rotationally impulsive. Formation of the ground vibrational state of the diatom is strongly favored at all wavelengths, but high-J rotational states are usually produced. These dynamical effects and the constraints of angular momentum conservation dictate that most of the available energy appear as fragment translation.

ACKNOWLEDGMENTS

This research is supported by the National Science Foundation through Grant No. CHE-8506010. J.J.V. gratefully acknowledges the receipt of a Faculty Research Grant from the University of California, Irvine in support of this work, the award of a Newly Appointed Faculty in Chemistry Grant by the Dreyfus Foundation, and a Cottrell Grant from the Research Corporation. J.J.V. also wishes to thank F. S. Rowland, J. A. Kaye, T. G. Slanger, R. D. Hudson, C. E. Kolb, and S. M. Anderson for helpful and stimulating discussions.

[1]World Meteorological Organization Global Ozone Research and Monitoring Project, Report No. 16, 1985.
[2]Jet Propulsion Laboratory, California Institute of Technology, Publication No. 85-37, 1985.
[3]R. G. Prinn, F. N. Alyea, and D. M. Cunnold, Annu. Rev. Earth Planet. Sci. **6**, 43 (1978).
[4]H. I. Schiff, Ann. Geophys. **28**, 67 (1972).
[5]P. J. Hay, R. T Pack, R. B. Walker, and E. J. Heller, J. Phys. Chem. **86**, 862 (1982).
[6]J. J. Valentini, Chem. Phys. Lett. **96**, 395 (1983).
[7]J. J. Valentini, J. Chem. Phys. **86**, 6757 (1987).
[8]H. B. Levene and J. J. Valentini, J. Chem. Phys. (submitted).
[9]For a review of CARS, see J. J. Valentini, in *Spectrometric Techniques*, edited by G. A. Vanasse (Academic, New York, 1985), Vol. 4, Chap. 1.
[10]A. A. Anda, D. L. Phillips, and J. J. Valentini, J. Chem. Phys. **85**, 1719 (1986).
[11]D. S. Moore, D. S. Bomse, and J. J. Vanlentini, J. Chem. Phys. **79**, 1745 (1983).
[12]K. P. Huber and G. Herzberg, *Molecular Spectra and Molecular Structure, IV. Constants of Diatomic Molecules* (Van Nostrand Reinhold, New York, 1979).
[13]J.-C. Nieh and J. J. Valentini, J. Phys. Chem. **91**, 91 (1987).
[14]See for example, F. T. Smith, Phys. Rev. **179**, 111 (1969).
[15]If the rotational wave functions for $O_2(^1\Delta_g)$ and $O_2(^3\Sigma_g)$ are strictly identical spherical harmonics appropriate to the rigid rotor, the selection rule will be $\Delta J = 0$, due to the orthogonality of the spherical harmonics. Whichever selection rule is appropriate, the effect is the same: for the $^{16}O^{16}O$ diatom only odd-J rotational states of $^1\Delta_g$ may cross due to the absence of even-J states in $^3\Sigma_g$.
[16]G. Herzberg, *Molecular Spectra and Molecular Structure, I. Spectra of Diatomic Molecules* (Van Nostrand Reinhold, New York, 1950).
[17]J. C. Brock and R. T. Watson, Chem. Phys. Lett. **71**, 371 (1980).
[18]R. K. Sparks, L. R. Carlson, K. Shobatake, M. L. Kowalczyk, and Y. T. Lee, J. Chem. Phys. **72**, 1401 (1980).
[19]See for example, R. Vasudev, R. N. Zare, and R. N. Dixon, J. Chem. Phys. **80**, 4863 (1984), and references therein.
[20]See for example, J. E. Heidenreich III and M. H. Thiemens, J. Chem. Phys. **78**, 892 (1983).
[21]J. C. Brock and R. T. Watson, Chem. Phys. **46**, 477 (1980).
[22]H. Okabe, *Photochemistry of Small Molecules* (Wiley, New York, 1978).
[23]E. Castellano and H. J. Schumacher, Chem. Phys. Lett. **13**, 625 (1972).
[24]H. B. Levene, J.-C. Nieh, and J. J. Valentini, J. Chem. Phys. (submitted).
[25]T. Tanaka and Y. Morino, J. Mol. Spectrosc. **33**, 538 (1970).
[26]R. H. Hughes, J. Chem. Phys. **24**, 131 (1956).
[27]Natl. Stand. Ref. Data. Ser., Natl. Bur. Stand. **37** (1971).